

# MagicDriveDiT: High-Resolution Long Video Generation for Autonomous Driving with Adaptive Control

Ruiyuan Gao<sup>1</sup>, Kai Chen<sup>2</sup>, Bo Xiao<sup>3</sup>, Lanqing Hong<sup>4</sup>, Zhenguo Li<sup>4</sup>, Qiang Xu<sup>1</sup>

<sup>1</sup>CUHK <sup>2</sup>HKUST <sup>3</sup>Huawei Cloud <sup>4</sup>Huawei Noah’s Ark Lab

{rygao, qxu}@cse.cuhk.edu.hk, kai.chen@connect.ust.hk,

{xiaobo15, honglanqing, li.zhenguo}@huawei.com

## Abstract

The rapid advancement of diffusion models has greatly improved video synthesis, especially in controllable video generation, which is vital for applications like autonomous driving. Although DiT with 3D VAE has become a standard framework for video generation, it introduces challenges in controllable driving video generation, especially for geometry control, rendering existing control methods ineffective. To address these issues, we propose MagicDriveDiT, a novel approach that integrates the MVDiT block and spatial-temporal conditional encoding to enable multi-view video generation and precise geometric control. Additionally, we introduce an efficient method for obtaining contextual descriptions for videos to support diverse textual control, along with a progressive training strategy using mixed video data to enhance training efficiency and generalizability. Consequently, MagicDriveDiT enables multi-view driving video synthesis with  $3.3\times$  resolution and  $4\times$  frame count (compared to current SOTA), rich contextual control, and geometric controls. Extensive experiments demonstrate MagicDriveDiT’s ability, unlocking broader applications in autonomous driving. Webpage: [flymin.github.io/magicdrivedit/](https://flymin.github.io/magicdrivedit/)

## 1. Introduction

The rapid advancements in diffusion models and controllable generation has substantially broadened its range of applications [19, 37]. Especially for autonomous driving, controllable generation of high-resolution and long videos has become a critical research focus [26, 41]. High resolution facilitates the identification of fine details [21], while long videos provide richer interaction for evaluating and improving algorithms [41]. These capabilities are indispensable for enhancing the performance and reliability of autonomous systems [11, 35]. However, due to limitations in model scalability and the compression capability of VAEs [2, 30], existing methods [11, 12] are significantly constrained by both resolution and frame count, as shown in Figure 1.

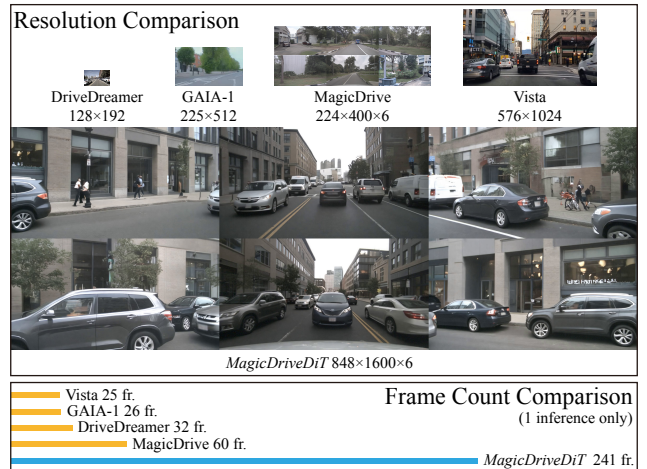


Figure 1. MagicDriveDiT generates high-resolution and long videos with multi-view and control supports, significantly exceeding the limitation of previous works [11, 12, 15, 35].

The introduction of DiT [29, 46] and 3D VAE [42, 46] has substantially alleviated these challenges. 3D VAE reduces computational overhead by performing spatial-temporal compression, effectively decreasing the computational cost of video generation by an order of magnitude. DiT enables quality improvements in generation with more model parameters and extensive data. Consequently, many text-to-video methods leverage DiT with 3D VAE for high-quality generation [42, 46]. However, autonomous driving requires multi-view generation with geometry control. How to effectively leverage the DiT with 3D VAE to achieve such controllable generation remains an open problem.

One of the most critical issue from controllable generation in autonomous driving is geometry control, which involves the positioning of objects and the road structures. These geometric conditions are typically time-dependent, meaning they correspond to individual video frames in a one-to-one manner. With 2D VAEs [2, 30], this characteristic allows control methods designed for images [43] to be seamlessly extended to video generation [11]. However, 3D VAE [42, 46] disrupts this alignment, as illustrated in

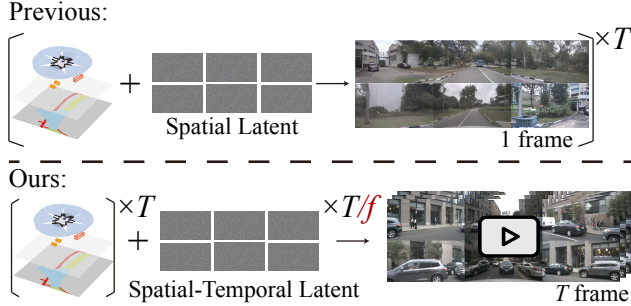


Figure 2. Different from spatial latent [11, 18, 26, 38, 39], spatial-temporal latent (ours) requires spatial-temporal condition injection for geometry controls (we omit the text condition here).

Figure 2. The spatial-temporal latent of 3D VAE requires that the control conditions also encapsulate corresponding spatial-temporal information. Therefore, it is necessary to redesign the geometry control module to accommodate the DiT with 3D VAE framework for driving video generation.

In this paper, we present *MagicDriveDiT*, a novel approach based on the DiT architecture, designed to tackle the challenges of high-resolution and long street-view video synthesis with precise control. Building upon DiT [29, 46] integrated with a 3D VAE for geometric control, we introduce an MVDiT block for multi-view video generation, and a novel spatial-temporal conditional encoding for latents derived from CogVAE [42], enabling precise management of geometric controls. Additionally, we enhance contextual description supports by efficiently generating captions for each video. To train the model efficiently, we employ a progressive training strategy, transitioning from short to long videos, which helps the model capture intricate details and generalize to complex scenarios. Furthermore, we utilize videos of diverse resolutions and durations to enhance the model’s generalization capability, enabling it to synthesize longer videos than those used in training.

Our *MagicDriveDiT* excels in generating highly realistic videos that align with text, road maps, 3D bounding boxes, and different camera perspectives, achieving significantly higher resolution and more frames than previous works (detailed in Table 1). Experiments and comparisons demonstrate the effectiveness of our training and control methods, significantly improving controllable street-view video synthesis. *MagicDriveDiT*’s flexibility in handling various resolutions, frames, and control signals enables the creation of novel street views suitable for simulations, expanding its potential applications across diverse domains.

In summary, the main contributions of this paper include:

- We design an efficient framework, *MagicDriveDiT*, leveraging progressive training to achieve high-quality, high-resolution, and long video generation (up to  $848 \times 1600 \times 6$ , 241 frames), significantly superior to prior works.
- For geometric controls, novel spatial-temporal control for objects, road semantics, and camera trajectories is pro-

Type	Method	Total Res.	Frame
Front View	GAIA-1*[15]	$288 \times 512 \times 1$	26
	DriveDreamer [35]	$128 \times 192 \times 1$	32
	Vista* [12]	$576 \times 1024 \times 1$	25
Multi-view	MagicDrive [11]	$224 \times 400 \times 6$	60
	Drive-WM [38]	$192 \times 384 \times 6$	8
	Panacea [39]	$256 \times 512 \times 6$	8
	DriveDreamer2 [45]	$256 \times 448 \times 6$	8
	Delphi [26]	$512 \times 512 \times 6$	10
	DiVE [18]	$480p \times 6$	16
	<i>MagicDriveDiT</i>	<b><math>848 \times 1600 \times 6</math></b>	<b>241</b>

Table 1. **Comparison of Resolution and Frame Count.** We only consider a single inference, since rollout notably degrades quality (see Appendix D). \*Only support text & image(s) conditions.

posed while maintaining multi-frame, multi-view consistency. For text control, we enrich the contextual description on driving datasets to support diverse generation.

- Our model generalizes well from image to video generation through mixed-resolution and duration training, with extrapolation capabilities, significantly exceeding the resolution and frame number in previous works.

## 2. Related Work

**Video Generation in Autonomous Driving.** Video generation is crucial for autonomous driving, with applications in training perception models [11], testing [41], and scene reconstruction [10, 44]. It demands extensive fields of view and dynamic object motion handling, requiring precise controllability [11] and high-resolution video production [21] with more frames [10] and multiple camera perspectives [44]. Diffusion models have improved controllable multi-view video generation, yet existing models [18, 26, 38, 39, 45] lack adequate resolution and frame count for policy testing [16] and data engine applications [10, 11, 44]. By achieving unprecedented resolution and frame count, as compared in Figure 1 and Table 1, *MagicDriveDiT* addresses the limitations of previous driving video generation methods, enabling more potential applications.

**Diffusion Models and DiT Architectures.** Diffusion models [13, 31, 47] generate data by learning the denoising steps from Gaussian noises to samples, widely used in image [8, 30, 37] and video [14] generation. From the modeling’s perspective, Flow Matching [9, 22] simplifies diffusion models, enhancing the efficiency of training and inference. From the implementation’s perspective, the architecture shifts from UNet [13] to DiT, due to better scalability [6, 29], especially for high-resolution tasks [5]. Our *MagicDriveDiT* also leverages Flow Matching and DiT for scaling to high-resolution and long video generation.

**Conditional Generation.** Conditional generation is crucial for various applications utilizing generative models. Cross-

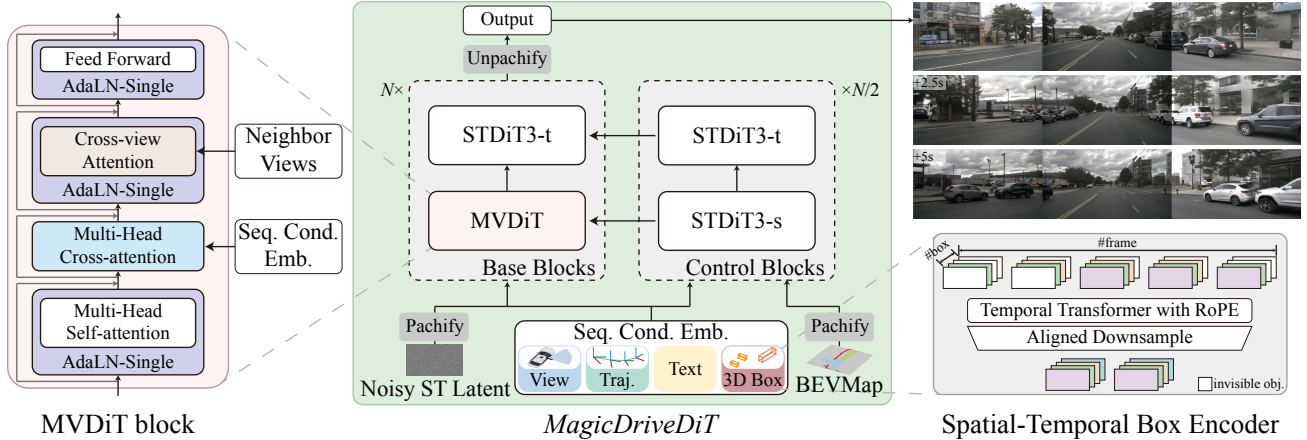


Figure 3. **Architecture Overview of *MagicDriveDiT***. To incorporate different conditions for video generation, *MagicDriveDiT* adopts a two-branch architecture as in [43] with basic STDiT3 blocks from [6, 46]. We propose the MVDiT block for multi-view consistency and Spatial-Temporal (Box/Traj.) Encoder to inject condition into the Spatial-Temporal (ST) Latent.

attention layers from LDM [30] and ControlNet’s [43] additive encoding for grid-shaped control signals are leading methods in controllable diffusion-based generation. In the street-view generation, *MagicDrive* [11] and *MagicDrive3D* [10] integrate 3D bounding boxes, BEV maps, ego trajectories, and camera poses for multi-view street scene synthesis. However, these methods are limited to spatial encoding and are not directly applicable to spatial-temporal latents from 3D VAE [42], as shown in Figure 2. *MagicDriveDiT* presents a novel control paradigm for spatial-temporally compressed latents from 3D VAE, enabling the controllable generation of high-resolution long videos.

### 3. Preliminary

**Problem Formulation.** This paper addresses controllable high-resolution and long video generation for street views. Given a sequence of frame descriptions  $\{\mathbf{S}_t\}, t \in \{0, \dots, T\}$ , the goal is to generate corresponding street-view videos from latent variables  $\mathbf{z} \sim \mathcal{N}(\mathbf{0}, \mathbf{I})$ , i.e.,  $\{\mathbf{I}_{c,t}\} = \mathcal{G}(\{\mathbf{S}_t\}, \mathbf{z})$ , where  $c \in \{0, \dots, C\}$  denotes the  $C$  camera views. Here, high resolution indicates that  $\mathbf{I}$  has a high resolution, and long video implies that  $T$  is large.

To describe a street-view video, we adopt the conditions outlined in [10, 11]. Specifically, frame descriptions  $\mathbf{S}_t = \{\mathbf{C}, \mathbf{M}_t, \mathbf{B}_t, \mathbf{L}, \mathbf{Tr}_t^0\}$  include the camera poses  $\{\mathbf{C}_c\} = [\mathbf{R}_c, \mathbf{t}_c]^1$ , a road map  $\mathbf{M}_t \in \{0, 1\}^{w \times h \times c}$  representing a  $w \times h$  meter road area in BEV with  $c$  semantic classes, 3D bounding boxes  $\mathbf{B}_t = \{(c_i, b_i)\}_{i=1}^N$  where each object is described by a box  $b_i = \{(x_j, y_j, z_j)\}_{j=1}^8 \in \mathbb{R}^{8 \times 3}$  and class  $c_i \in \mathcal{C}$ , text  $\mathbf{L}$  adding information for the whole video (e.g., weather and time of day), and the ego vehicle trajectory  $\mathbf{Tr}_t^0$  which describes the transformation from the LiDAR coordinate of each frame to the first frame, i.e.,

<sup>1</sup>Typically, cameras are fixed throughout the video.

$\mathbf{Tr}_t^0 = [\mathbf{R}_t^0, \mathbf{t}_t^0]$ . All geometric data, except  $\mathbf{Tr}_t^0$ , is parameterized in the ego car’s local LiDAR frame.

**LDMs and Flow Matching.** For high-resolution image generation, Rombach et al. [30] propose Latent Diffusion Models (LDMs), using a pre-trained VAE for image down-sampling and diffusion models for latent generation. This manner is widely adopted in both image generation [6, 9] and video generation [2, 3, 46]. *MagicDriveDiT* is also based on the VAE+diffusion formulation. With the latest advancement on diffusion models, Esser et al. [9] propose to train large scale diffusion models through simulation-free rectified flow [23, 24] and v-prediction loss [9]:

$$\mathbf{z}_t = (1 - t)x_0 + t\epsilon \quad (1)$$

$$\mathcal{L}_{CFM} = \mathbb{E}_{\epsilon \sim \mathcal{N}(0, \mathbf{I})} \|v_{\Theta}(\mathbf{z}_t, t) - \frac{1}{1-t}(\mathbf{z} - \epsilon)\|_2^2, \quad (2)$$

where  $t \sim \text{lognorm}(0, 1)$  is timestep and  $v_{\Theta}$  is the model.

## 4. Methods

### 4.1. Overview of *MagicDriveDiT*

Figure 3 illustrates an overview of the model architecture. Based on the STDiT-3 blocks Zheng et al. [46], we introduce Multi-View DiT (MVDiT) block for multi-view generation and employ cross-attention [30] for text, boxes, camera views, and trajectories, alongside an additive branch [43] for maps to inject control signals.

Nevertheless, the spatial encoding of control signals [11, 26, 38, 39, 45] is incompatible with spatial-temporal latents, as illustrated in Figure 2. Consequently, the encoder for each control signal is reformulated, exemplified by the spatial-temporal box encoder on the right of Figure 3. Further details are provided in Section 4.3.

Besides, *MagicDriveDiT* enriches text control beyond previous works (e.g. [11]) by generating contextual descrip-

tion through image captioning (Section 4.4). Furthermore, *MagicDriveDiT* employs progressive training from images to high-resolution short videos, then to long videos, enhancing diffusion model convergence. Using variable-length, multi-resolution videos in training also enables image and video generation at diverse resolutions and frame extrapolation beyond training settings (Section 4.5).

## 4.2. Architecture for High-Resolution Long Video

Training high-resolution, long-video diffusion models is computationally intensive, requiring significant GPU memory. DiT and 3D VAE are key to scaling these models. As noted by Peebles and Xie [29], DiT’s lower Gflops correlate with better FID, making it more efficient than UNet [11]. For memory, 3D VAE [42] compresses temporal information by 4×, achieving a 256× compression ratio<sup>2</sup>, reducing sequence length and memory use, especially for transformers [7]. Architectural unification [34] enables DiT to leverage advanced parallelization, *e.g.*, sequence parallelism [46], overcoming single GPU memory limits for higher resolution and longer videos.

As depicted in Figure 3, *MagicDriveDiT* utilizes STDiT-3 blocks as per Zheng et al. [46]. The architecture design incorporates two significant modifications. First, to facilitate multi-view generation, the Multi-View DiT (MVDiT) block integrates a cross-view attention layer [11], as shown on the left of Figure 3. Second, given the need for handling multiple control elements, *MagicDriveDiT* employs cross-attention [30] for text, boxes, camera views, and trajectories, alongside an additive branch [43] for maps to inject control signals.

## 4.3. Spatial-Temporal Control on 3D VAE

A major challenge with 3D VAE adoption is geometric control. As in Figure 2, geometric control manages per-frame content spatially. Previously with 2D VAE, the temporal axis persists in geometric descriptors  $\{\mathbf{S}_t\}, t \in \{1, \dots, T\}$ , video latent and the decoded video. This temporally aligning feature enables video geometric control with spatial control methods similar to that on images [27]. However, 3D VAE yields  $T/f$  latents (where  $f$  is the temporal compression ratio), misaligning control signals with latents and rendering previous control techniques [11, 39] ineffective.

Besides, the issue of temporal misalignment does not exist in ambiguous control conditions (*e.g.*, text), as these conditions are typically employed to describe the entire video. Specifically, the temporal dimension of such conditions is 1, and they are repeated for  $T/f$  times to control the entire video. Consequently, a naive approach to handle such dimension misalignment would be to follow the method of text control, where the temporal dimension is first reduced to 1 through a temporal encoder and then repeated to  $T/f$

<sup>2</sup>We ignore latent dimension discrepancies.

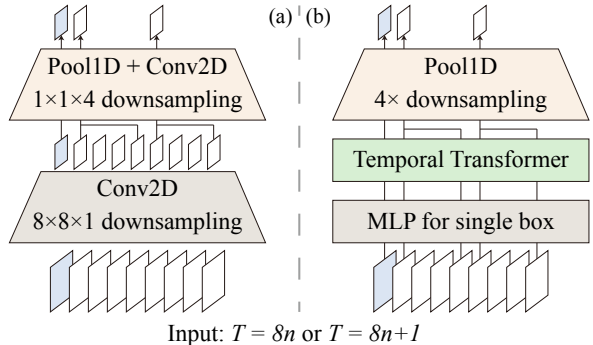


Figure 4. **Spatial-Temporal Encoder for Maps (a) and Boxes (b).** Our spatial encoding module follows [11], and temporal encoding integrates the downsampling strategy in our 3D VAE [42], resulting in temporally aligned embedding between the control signals and video latents.

for control. However, our experiments reveal that this operation results in trailing issues (as “Box Reduce” in Figure 10), which we hypothesize are caused by the repeat operation. Therefore, we design a downsampling method that aligns the dimensions while preserving the distinctiveness of temporal information, thereby enabling precise control of geometric information for each frame.

Our spatial-temporal encoding modules are illustrated in Figure 4. This involves re-aligning the maps ( $\mathbf{M}_t$ ), boxes ( $\mathbf{B}_t$ ), and trajectory ( $\mathbf{Tr}_t^0$ ) within the scene descriptor ( $\mathbf{S}_t$ ). Maps, represented as grid data, are straightforward to manage. By extending ControlNet’s [43] design, we utilize temporal downsampling modules with new trainable parameters in 3D VAE to align features between control and base blocks, as depicted in Figure 4(a).

For 3D boxes, padding is applied to invisible boxes to maintain consistent box sequence length across views and frames, illustrated in Figure 3 right. We employ a downsampling module with a temporal transformer and RoPE [32] to capture temporal correlation, creating spatial-temporal embeddings aligned with video latents, as in Figure 4(b). The spatial-temporal encoder for boxes can also be adapted for ego trajectory ( $\mathbf{Tr}_t^0$ ), by replacing the MLP for boxes with an MLP for camera poses [11].

All the downsampling ratios are aligned with the adopted 3D VAE [42], *i.e.*, with  $8n$  or  $8n + 1$  as inputs, and  $2n$  or  $2n + 1$  as outputs, respectively. Section 5.3 holds more ablation studies on different downsampling methods.

## 4.4. Enrich Text Control by Image Caption

Although geometric descriptors offer precise control over objects and maps, textual descriptions in autonomous driving datasets (*e.g.*, nuScenes) are often restricted to basic weather (sunny/rain) and time (day/night), lacking richer scene context such as road types (*e.g.*, highway/urban) or background elements (*e.g.*, buildings, trees). To enhance textual control, we regenerated video captions using a Mul-



Figure 5. *MagicDriveDiT* supports more diverse text control by enriching the textual description of driving datasets (e.g., nuScene [4], Waymo [33]) than previous works (e.g., [11]). Please see the full videos on our project page.

timodal Large Language Model (MLLM) [17]. By prompting MLLM to focus on aspects beyond object categories, trajectories, and road structures, we ensure efficiency and consistency. Specifically, first, it eliminates the need for the MLLM to describe dynamics, thus only the middle frame of each video is used; second, it avoids potential conflicts between multiple control signals. Figure 5 shows the diverse contextual description supports of *MagicDriveDiT*.

#### 4.5. Progressive Training with Mixed Video Types

To accelerate model convergence, we employ a three-stage training strategy: starting with low-resolution images, transitioning to high-resolution short videos, and finally using high-resolution long videos. This approach is based on two key insights. First, in controllable generation, models prioritize content quality before learning controllability, also observed by Gao et al. [12]. Our progressive training enables faster controllability acquisition. Second, models adapt more quickly to high resolution than to long videos, so we emphasize short-video training early on. Details of the mixing method are provided in the Appendix B.

In the third stage, we mix videos up to 241 frames (the maximum frame count of the dataset) at  $224 \times 400$  and a resolution of up to  $848 \times 1600$  (the maximum resolution of nuScenes [4]) at 33 frames. This mixed-resolution and mixed-length training allows the model to generalize across dimensions, supporting flexible generation and extrapolation beyond training configurations (e.g., up to  $848 \times 1600$  at 241 frames as demonstrated in Section 6). Ablation studies in Section 5.3 further validate this approach.

## 5. Experiments

### 5.1. Experimental Setups

**Dataset and Baselines.** We employ the nuScenes dataset [4], a prominent dataset for street-view genera-

Method	FVD↓	mAP↑	mIoU↑
MagicDrive [11] (16f)	218.12	11.86	18.34
MagicDrive [11] (60f)	217.94	11.49	18.27
MagicDrive3D [10]	210.40	12.05	18.27
<i>MagicDriveDiT</i>	<b>94.84</b>	<b>18.17</b>	<b>20.40</b>

Table 2. **Comparison with Baselines for Controllable Video Generation.** Videos are generated according to conditions from the nuScenes validation set. Only first 16 frames are kept for evaluation, as in [28]. ↑/↓ indicates that a higher/lower value is better.

tion [11, 26, 40], to evaluate *MagicDriveDiT*. We adhere to the official splits, using 700 multi-view videos for training and 150 for validation. Our primary baseline is MagicDrive [11], comprising three models: MagicDrive (16f) for 16-frame video generation; MagicDrive (60f), which extends MagicDrive (16f) to 60 frames, both from Gao et al. [11]; and MagicDrive3D, a 16-frame model from Gao et al. [10]. Moreover, we employed the Waymo Open Dataset [33] to further fine-tune the model, aiming to validate its scalability and to facilitate the generation of videos with diverse environmental styles and different numbers of perspectives. Further details are provided in Appendix D.

**Evaluation Metrics.** We evaluate both realism and controllability in street-view generation for videos and images. For video generation, we follow benchmarks from [28], utilizing FVD for video quality; mAP from 3D object detection and mIoU from BEV segmentation for controllability, using BEVFormer [20] for both tasks, which is a video-based perception model. For image generation, we adopt the metrics from Gao et al. [11], employing FID for image quality; mAP with BEVFusion [25] and road mIoU with CVT [48] for controllability assessment. BEVFusion and CVT are image-based models.

**Model Setup.** In accordance with Section 4.2, we adopt the 3D VAE framework from CogVideoX [42] and train diffusion models for street-view video generation from scratch<sup>3</sup>. Initially, the model comprises only spatial blocks for base and control blocks, focusing on image generation. Temporal blocks are incorporated in the second stage, forming the full architecture of *MagicDriveDiT*. Further training details can be found in Appendix E.

### 5.2. Results and Analysis

**Generation Quality.** *MagicDriveDiT* excels in both video and image generation tasks. In video tasks, it significantly reduces FVD compared to MagicDrive (Table 2), due to the DiT architecture enhancing inter-frame consistency and spatial-temporal condition encoding for precise control of object motion and positioning. Further illustrated in Figure 6, *MagicDriveDiT* generates high-resolution videos that

<sup>3</sup>For more discussion on this choice, see Section 5.3 and Appendix H.



Figure 6. **Qualitative Comparison between *MagicDriveDiT* and *MagicDrive* [11]**. Frames are extracted from the generated videos. To conserve space, we only present the 3 (out of 6) perspectives that include the front view. Two crops from the generated views are magnified and shown on the right. By generating  $4\times$  resolution of *MagicDrive*, the synthesized street view of our model contains finer details.

not only improve quality but also incorporate more intricate details, closely resembling footage captured by real cameras. This enhancement is achieved through our advanced training on variable lengths and resolutions, allowing for more realistic and detailed outputs. We further conduct human evaluation on consistency in Appendix F.

Beneficial from the mixing training approach, *MagicDriveDiT* is capable of image generation. As shown in Table 3, *MagicDriveDiT* matches baseline performance in multi-view street-view tasks and surpasses baselines in vehicle segmentation mIoU and object detection mAP. This demonstrates the strong generalization capabilities of our spatial-temporal condition encoding.

**Controllability.** The quantitative results presented in Table 2 and 3 demonstrate that the images and videos generated by *MagicDriveDiT* effectively reflect the control conditions. Additionally, Figure 5 and 8 provide visual results, showing that multiple control conditions can independently influence the generated content. For instance, weather can be altered via text input (from sunny to rainy) while maintaining road structure, and the trajectories of other vehicles and the ego vehicle. By varying the combinations of conditions, *MagicDriveDiT* is capable of producing a diverse range of high-quality street-view videos.

### 5.3. Ablation Studies

**VAE Comparison for Street Views.** Before training the diffusion models, we evaluate the performance of open-source 3D VAEs (*i.e.*, CogVAE [42] and Open-Sora [46]) on street views, in comparison with the 2D SD VAE [30]. As illustrated in Figure 7, CogVAE consistently outperforms its counterparts on reconstruction ability. Besides, as presented in Appendix G, CogVAE demonstrates minimal performance degradation over longer video sequences, making

Method	FID ↓	Road mIoU↑	Vehicle mIoU↑	mAP ↑
BEVControl [40]	24.85	60.80	26.80	N/A
MagicDrive [11] (Img)	<b>16.20</b>	<b>61.05</b>	27.01	12.30
<i>MagicDriveDiT</i>	20.91	59.79	<b>32.73</b>	<b>17.65</b>

Table 3. **Comparison with Baselines for Controllable Image Generation.** All the annotations & camera views from the nuScenes validation set are used for evaluation.  $\uparrow/\downarrow$  indicates that a higher/lower value is better.



Figure 7. **Reconstruction Visualization from Different VAEs.** CogVAE [42] maintains most details compared with others and exhibits better performance for high-resolution content.

it particularly well-suited for long video generation tasks. Additionally, we found that all VAEs exhibit improved reconstruction capabilities with increasing resolution. This insight is beneficial for advancing our model’s ability to generate high-quality images and videos by focusing on higher-resolution outputs. For more detailed quantitative results and discussion, see Appendix G.

**Spatial-Temporal Conditioning.** We demonstrate the spatial-temporal encoder’s effectiveness by the validation loss in over-fitting experiments (Figure 9) and visualization comparison (Figure 10). We compare two baselines:

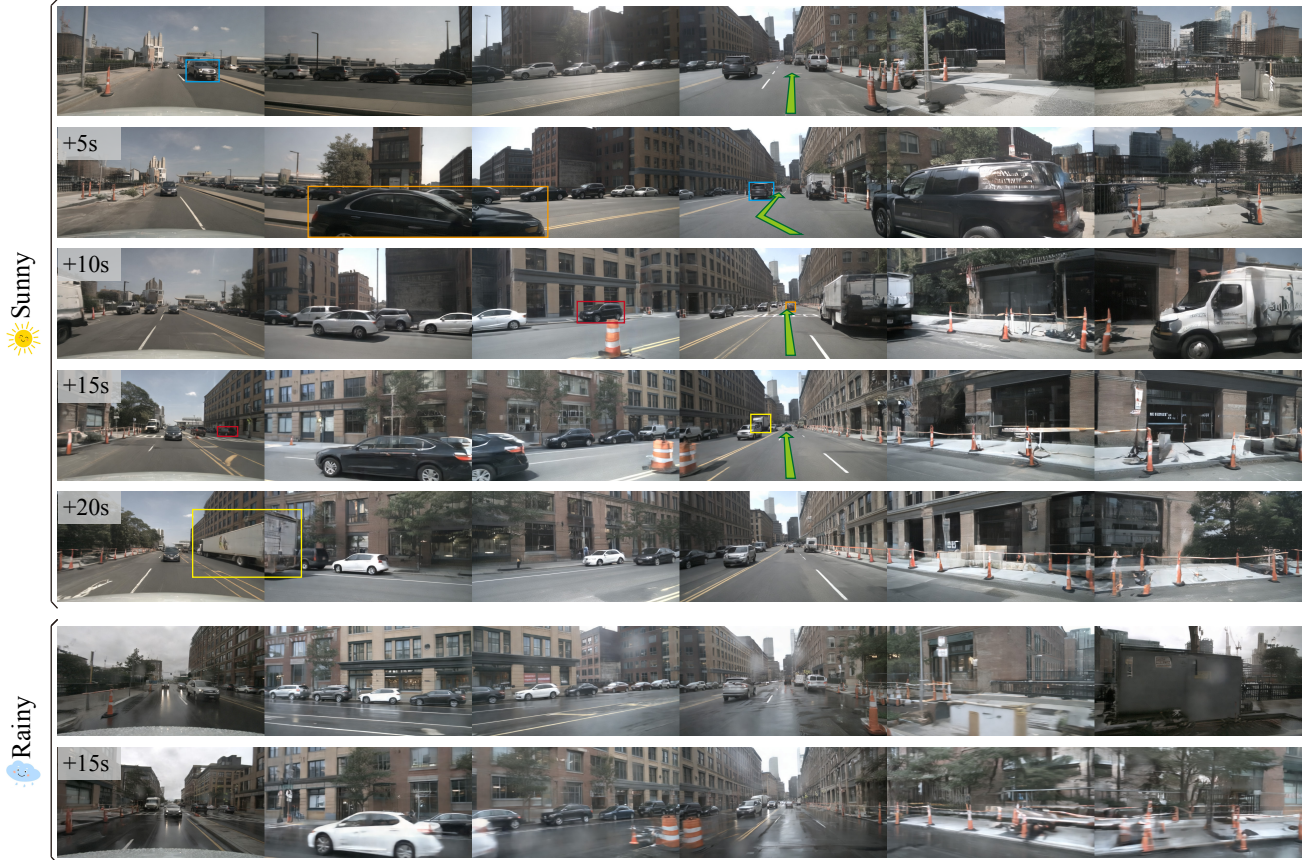


Figure 8. *MagicDriveDiT* generates high-resolution (e.g.,  $424 \times 800$  here) street-view videos for 241 frames (i.e., the full length of nuScenes videos, approximately 20 seconds at 12 FPS) with multiple controls (i.e., road map, object boxes, ego trajectory, and text). Notably, the 241-frame length at  $424 \times 800$  is unseen during training, demonstrating our method’s generalization capability to video length. We annotate the ego-vehicle trajectory and selected objects to aid localization, with same-color boxes denoting the same object. Due to space constraints, the “rainy” example includes only two frames; additional examples can be found in Appendix J and on our project page.

global temporal dimension reduction (Reduce) and temporal dimension interpolation (Interp.) for alignment. In over-fitting training with 16 samples, the  $4 \times$  downsampling technique ( $4 \times$  down, ours) accelerates convergence and achieves the lowest final validation loss [9], as shown in Figure 9. Furthermore, Figure 10 illustrates that, unlike the global reduction baseline,  $4 \times$  down reduces artifacts and maintains accurate motion trajectories. These results confirm the spatial-temporal encoder’s capability to enhance data encoding and improve video generation performance using spatial-temporal latents.

**Variable Length and Resolution Training.** As presented in Section 4.5, *MagicDriveDiT* adopts a training strategy by mixing different length and resolution videos. Our ablation study demonstrates the effectiveness of this strategy. As shown in Table 4, the limitations of VAE (as discussed in Section 5.2) are evident when using only low-resolution videos ( $17 \times 224 \times 400$ ), indicated by worse FVD and lower mAP and mIoU scores compared to other settings. Incorporating longer videos improves the model’s controllability

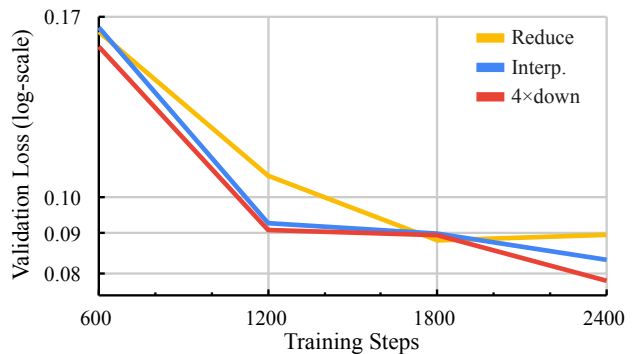


Figure 9. **Validation Loss through Training with Different ST Encodings.**  $4 \times$ down (our methods in *MagicDriveDiT*) can help the model converge, performing the best among all the encodings.

(both mAP and mIoU are higher), while incorporating high-resolution videos enhances overall quality (all three metrics are notably improved).

Although mixing different frame lengths slightly degrades FVD, it is crucial for enabling the model to generate videos of various lengths and extrapolate to unseen lengths

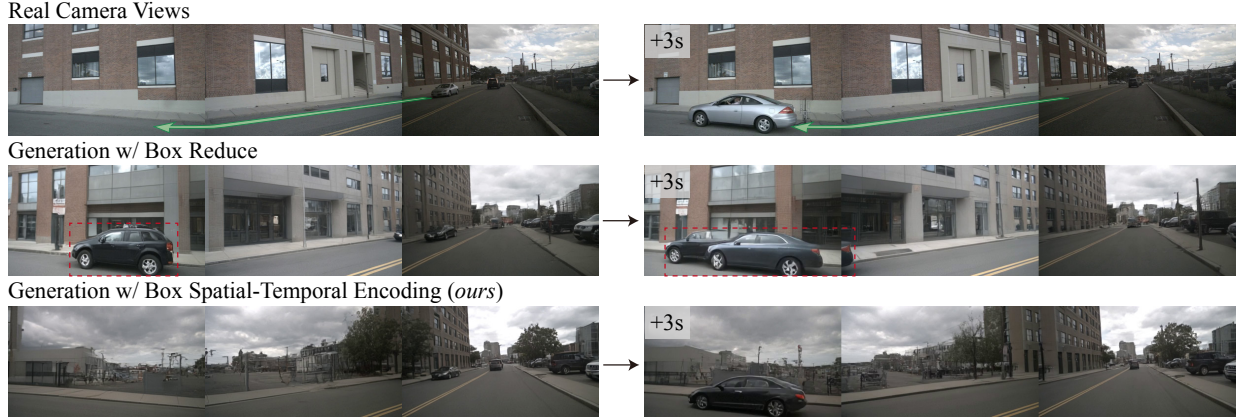


Figure 10. **Visual Effect of Spatial-Temporal Encoding for Boxes.** For videos with spatial-temporal latent encoding, a simple global reduce baseline can cause artifacts and trailing effects in object trajectories across viewpoints (we highlight them with red boxes). Our spatial-temporal encoding effectively resolves this, maintaining object clarity and accurate motion trajectories.

Training Data	FVD↓	mAP↑	mIoU↑
17×224×400	97.21	10.17	12.42
(1-65)-224×400	100.73	10.51	12.74
17×(224×440 - 424×800)	<b>96.34</b>	14.91	17.53
1-65×(224×440 - 424×800)	99.66	<b>15.44</b>	<b>18.26</b>

Table 4. **Comparison between Different Training Configurations.** To test adaptation ability for higher resolution and longer videos, all the models load a pre-trained weight for short videos (9×424×800) and are trained with the same GPU hours.

(see Section 6). Thus, we combine both resolutions and frame lengths, effectively balancing the trade-offs between video quality, controllability, and model functionality.

## 6. Applications

**Extrapolation for Longer Video Generation.** Through variable length and resolution training (Section 4.5), *MagicDriveDiT* effectively generates videos exceeding the training setup’s length. Though trained on videos up to 33×848×1600 and 241×224×400, *MagicDriveDiT* successfully produces 241×848×1600 videos (full length and full resolution of nuScenes), which are 8× the length of the training samples, as demonstrated in Figure 8 and videos on our project page. To further validate this capability, we compare the first-16-frame FVD for short videos (17 frames) and per-16-frame FVD for longer videos (65 frames and above). As shown in Table 5, the 16-frame FVDs remain consistent across both seen and extrapolated configurations, extending to 129×848×1600×6 generation (this is not the upper limit; please see note in the Appendix). This affirms the model’s robust generalization capability.

**Fast Generalization on Other Datasets.** To evaluate the generalization of *MagicDriveDiT*, we fine-tuned the Stage 3 model on the Waymo dataset [33], enabling rapid generation of 3-view videos in 1 day (1k+ steps) with strong con-

Resolution	First-16-Frame	Avg. of Per-16-Frame		
		2×	3×	4×
424×800	530.65	562.99	/	/
848×1600	559.70	573.46	583.50	585.89

Table 5. **Generation Quality for Videos Longer than Training.** We randomly sample 10 sequences from the nuScenes validation set and report FVD (the lower the better).  $n\times$ :  $n$  times of maximum training frame number, *i.e.*, 129 frames for 424×800 and 33 for 848×1600. /: exceed the maximum frame of dataset.

trollability (examples shown in Figure 5 and more videos can be found on our project page). Moreover, mixed training on Waymo and nuScenes datasets further enhanced the model’s ability to generate videos with varying perspectives, improving overall quality. The final model achieved an FVD of 105.17 on Waymo and 74.30 on nuScenes, surpassing results in Table 2.

## 7. Conclusion and Discussion

In this paper, we presented *MagicDriveDiT*, an innovative framework for high-resolution and long video synthesis with precise control, specifically tailored for applications like autonomous driving. By introducing MVDiT block and spatial-temporal conditional encoding module, *MagicDriveDiT* effectively addresses the challenges of scalability and geometry control in video generation with the DiT architecture and 3D VAE. Our approach also introduces richer contextual description for driving video generation, and a progressive training strategy with variable length and resolution adaption, enhancing the model’s generation ability. Extensive experiments demonstrate that *MagicDriveDiT* generates realistic videos that maintain spatial and temporal coherence, significantly surpassing previous methods in resolution and frame count, opening new possibilities for simulations and other applications in autonomous driving.

## References

- [1] Niket Agarwal, Arslan Ali, Maciej Bala, Yogesh Balaji, Erik Barker, Tiffany Cai, Prithvijit Chattopadhyay, Yongxin Chen, Yin Cui, Yifan Ding, et al. Cosmos world foundation model platform for physical ai. *arXiv preprint arXiv:2501.03575*, 2025. 3
- [2] Andreas Blattmann, Tim Dockhorn, Sumith Kulal, Daniel Mendelevitch, Maciej Kilian, Dominik Lorenz, Yam Levi, Zion English, Vikram Voleti, Adam Letts, et al. Stable video diffusion: Scaling latent video diffusion models to large datasets. *arXiv preprint arXiv:2311.15127*, 2023. 1, 3
- [3] Tim Brooks, Bill Peebles, Connor Holmes, Will DePue, Yufei Guo, Li Jing, David Schnurr, Joe Taylor, Troy Luhman, Eric Luhman, Clarence Ng, Ricky Wang, and Aditya Ramesh. Video generation models as world simulators. 2024. 3
- [4] Holger Caesar, Varun Bankiti, Alex H. Lang, Sourabh Vora, Venice Erin Liang, Qiang Xu, Anush Krishnan, Yu Pan, Giancarlo Baldan, and Oscar Beijbom. nuscenes: A multi-modal dataset for autonomous driving. In *CVPR*, 2020. 5, 2
- [5] Junsong Chen, Chongjian Ge, Enze Xie, Yue Wu, Lewei Yao, Xiaozhe Ren, Zhongdao Wang, Ping Luo, Huchuan Lu, and Zhenguo Li. Pixart- $\sigma$ : Weak-to-strong training of diffusion transformer for 4k text-to-image generation. In *ECCV*, 2024. 2
- [6] Junsong Chen, Jincheng Yu, Chongjian Ge, Lewei Yao, Enze Xie, Zhongdao Wang, James Kwok, Ping Luo, Huchuan Lu, and Zhenguo Li. Pixart- $\alpha$ : Fast training of diffusion transformer for photorealistic text-to-image synthesis. In *ICLR*, 2024. 2, 3
- [7] Tri Dao, Daniel Y. Fu, Stefano Ermon, Atri Rudra, and Christopher Ré. FlashAttention: Fast and memory-efficient exact attention with IO-awareness. In *NeurIPS*, 2022. 4
- [8] Prafulla Dhariwal and Alexander Nichol. Diffusion models beat gans on image synthesis. In *NeurIPS*, 2021. 2
- [9] Patrick Esser, Sumith Kulal, Andreas Blattmann, Rahim Entezari, Jonas Müller, Harry Saini, Yam Levi, Dominik Lorenz, Axel Sauer, Frederic Boesel, et al. Scaling rectified flow transformers for high-resolution image synthesis. In *ICML*, 2024. 2, 3, 7
- [10] Ruiyuan Gao, Kai Chen, Zhihao Li, Lanqing Hong, Zhenguo Li, and Qiang Xu. Magicdrive3d: Controllable 3d generation for any-view rendering in street scenes. *arXiv preprint arXiv:2405.14475*, 2024. 2, 3, 5
- [11] Ruiyuan Gao, Kai Chen, Enze Xie, HONG Lanqing, Zhenguo Li, Dit-Yan Yeung, and Qiang Xu. Magicdrive: Street view generation with diverse 3d geometry control. In *ICLR*, 2024. 1, 2, 3, 4, 5, 6
- [12] Shenyan Gao, Jiazhi Yang, Li Chen, Kashyap Chitta, Yihang Qiu, Andreas Geiger, Jun Zhang, and Hongyang Li. Vista: A generalizable driving world model with high fidelity and versatile controllability. *arXiv preprint arXiv:2405.17398*, 2024. 1, 2, 5, 3, 4
- [13] Jonathan Ho, Ajay Jain, and Pieter Abbeel. Denoising diffusion probabilistic models. In *NeurIPS*, 2020. 2
- [14] Jonathan Ho, Tim Salimans, Alexey Gritsenko, William Chan, Mohammad Norouzi, and David J Fleet. Video diffusion models. In *NeurIPS*, 2022. 2
- [15] Anthony Hu, Lloyd Russell, Hudson Yeo, Zak Murez, George Fedoseev, Alex Kendall, Jamie Shotton, and Gianluca Corrado. Gaia-1: A generative world model for autonomous driving. *arXiv preprint arXiv:2309.17080*, 2023. 1, 2
- [16] Yihan Hu, Jiazhi Yang, Li Chen, Keyu Li, Chonghao Sima, Xizhou Zhu, Siqi Chai, Senyao Du, Tianwei Lin, Wenhai Wang, Lewei Lu, Xiaosong Jia, Qiang Liu, Jifeng Dai, Yu Qiao, and Hongyang Li. Planning-oriented autonomous driving. In *CVPR*, 2023. 2
- [17] Aaron Hurst, Adam Lerer, Adam P Goucher, Adam Perelman, Aditya Ramesh, Aidan Clark, AJ Ostrow, Akila Welihinda, Alan Hayes, Alec Radford, et al. Gpt-4o system card. *arXiv preprint arXiv:2410.21276*, 2024. 5
- [18] Junpeng Jiang, Gangyi Hong, Lijun Zhou, Enhui Ma, Hengtong Hu, Xia Zhou, Jie Xiang, Fan Liu, Kaicheng Yu, Haiyang Sun, et al. Dive: Dit-based video generation with enhanced control. *arXiv preprint arXiv:2409.01595*, 2024. 2
- [19] Pengxiang Li, Kai Chen, Zhili Liu, Ruiyuan Gao, Lanqing Hong, Guo Zhou, Hua Yao, Dit-Yan Yeung, Huchuan Lu, and Xu Jia. Trackdiffusion: Tracklet-conditioned video generation via diffusion models. In *WACV*, 2025. 1
- [20] Zhiqi Li, Wenhai Wang, Hongyang Li, Enze Xie, Chonghao Sima, Tong Lu, Yu Qiao, and Jifeng Dai. Bevformer: Learning bird’s-eye-view representation from multi-camera images via spatiotemporal transformers. In *ECCV*, 2022. 5
- [21] Tingting Liang, Hongwei Xie, Kaicheng Yu, Zhongyu Xia, Zhiwei Lin, Yongtao Wang, Tao Tang, Bing Wang, and Zhi Tang. BEVFusion: A Simple and Robust LiDAR-Camera Fusion Framework. In *NeurIPS*, 2022. 1, 2
- [22] Yaron Lipman, Ricky TQ Chen, Heli Ben-Hamu, Maximilian Nickel, and Matthew Le. Flow matching for generative modeling. In *ICLR*, 2023. 2
- [23] Yaron Lipman, Ricky T. Q. Chen, Heli Ben-Hamu, Maximilian Nickel, and Matthew Le. Flow matching for generative modeling. In *ICLR*, 2023. 3
- [24] Xingchao Liu, Chengyue Gong, et al. Flow straight and fast: Learning to generate and transfer data with rectified flow. In *ICLR*, 2023. 3
- [25] Zhijian Liu, Haotian Tang, Alexander Amini, Xingyu Yang, Huizi Mao, Daniela Rus, and Song Han. Bevfusion: Multi-task multi-sensor fusion with unified bird’s-eye view representation. In *ICRA*, 2023. 5
- [26] Enhui Ma, Lijun Zhou, Tao Tang, Zhan Zhang, Dong Han, Junpeng Jiang, Kun Zhan, Peng Jia, Xianpeng Lang, Haiyang Sun, et al. Unleashing generalization of end-to-end autonomous driving with controllable long video generation. *arXiv preprint arXiv:2406.01349*, 2024. 1, 2, 3, 5
- [27] Chenlin Meng, Yutong He, Yang Song, Jiaming Song, Jiajun Wu, Jun-Yan Zhu, and Stefano Ermon. SDEdit: Guided image synthesis and editing with stochastic differential equations. In *ICLR*, 2022. 4
- [28] W-CODA2024 Organizers. Track 2: Corner case scene generation - multimodal perception and comprehension of corner cases in autonomous driving, 2024. 5

- [29] William Peebles and Saining Xie. Scalable diffusion models with transformers. In *ICCV*, 2023. 1, 2, 4
- [30] Robin Rombach, Andreas Blattmann, Dominik Lorenz, Patrick Esser, and Björn Ommer. High-resolution image synthesis with latent diffusion models. In *CVPR*, 2022. 1, 2, 3, 4, 6
- [31] Yang Song, Jascha Sohl-Dickstein, Diederik P Kingma, Abhishek Kumar, Stefano Ermon, and Ben Poole. Score-based generative modeling through stochastic differential equations. In *ICLR*, 2020. 2
- [32] Jianlin Su, Murtadha Ahmed, Yu Lu, Shengfeng Pan, Wen Bo, and Yunfeng Liu. Roformer: Enhanced transformer with rotary position embedding. *Neurocomputing*, 568:127063, 2024. 4
- [33] Pei Sun, Henrik Kretschmar, Xerxes Dotiwalla, Aurelien Chouard, Vijaysai Patnaik, Paul Tsui, James Guo, Yin Zhou, Yuning Chai, Benjamin Caine, Vijay Vasudevan, Wei Han, Jiquan Ngiam, Hang Zhao, Aleksei Timofeev, Scott Ettinger, Maxim Krivokon, Amy Gao, Aditya Joshi, Yu Zhang, Jonathon Shlens, Zhifeng Chen, and Dragomir Anguelov. Scalability in perception for autonomous driving: Waymo open dataset. In *CVPR*, 2020. 5, 8, 2
- [34] Peize Sun, Yi Jiang, Shoufa Chen, Shilong Zhang, Bingyue Peng, Ping Luo, and Zehuan Yuan. Autoregressive model beats diffusion: Llama for scalable image generation. *arXiv preprint arXiv:2406.06525*, 2024. 4
- [35] Xiaofeng Wang, Zheng Zhu, Guan Huang, Xinze Chen, Jiagan Zhu, and Jiwen Lu. Drivedreamer: Towards real-world-driven world models for autonomous driving. *arXiv preprint arXiv:2309.09777*, 2023. 1, 2
- [36] Xiaofeng Wang, Zheng Zhu, Yunpeng Zhang, Guan Huang, Yun Ye, Wenbo Xu, Ziwei Chen, and Xingang Wang. Are we ready for vision-centric driving streaming perception? the asap benchmark. In *CVPR*, 2023. 2
- [37] Yibo Wang, Ruiyuan Gao, Kai Chen, Kaiqiang Zhou, Yingjie Cai, Lanqing Hong, Zhenguo Li, Lihui Jiang, Dit-Yan Yeung, Qiang Xu, et al. Detdiffusion: Synergizing generative and perceptive models for enhanced data generation and perception. In *CVPR*, 2024. 1, 2
- [38] Yuqi Wang, Jiawei He, Lue Fan, Hongxin Li, Yuntao Chen, and Zhaoxiang Zhang. Driving into the future: Multiview visual forecasting and planning with world model for autonomous driving. In *CVPR*, 2024. 2, 3
- [39] Yuqing Wen, Yucheng Zhao, Yingfei Liu, Fan Jia, Yanhui Wang, Chong Luo, Chi Zhang, Tiancai Wang, Xiaoyan Sun, and Xiangyu Zhang. Panacea: Panoramic and controllable video generation for autonomous driving. In *CVPR*, 2024. 2, 3, 4
- [40] Kairui Yang, Enhui Ma, Jibin Peng, Qing Guo, Di Lin, and Kaicheng Yu. Bevcontrol: Accurately controlling street-view elements with multi-perspective consistency via bev sketch layout. *arXiv preprint arXiv:2308.01661*, 2023. 5, 6
- [41] Xuemeng Yang, Licheng Wen, Yukai Ma, Jianbiao Mei, Xin Li, Tiantian Wei, Wenjie Lei, Daocheng Fu, Pinlong Cai, Min Dou, et al. Drivearena: A closed-loop generative simulation platform for autonomous driving. *arXiv preprint arXiv:2408.00415*, 2024. 1, 2
- [42] Zhuoyi Yang, Jiayan Teng, Wendi Zheng, Ming Ding, Shiyu Huang, Jiazheng Xu, Yuanming Yang, Wenyi Hong, Xiaohan Zhang, Guanyu Feng, et al. Cogvideox: Text-to-video diffusion models with an expert transformer. *arXiv preprint arXiv:2408.06072*, 2024. 1, 2, 3, 4, 5, 6
- [43] Lvmin Zhang, Anyi Rao, and Maneesh Agrawala. Adding conditional control to text-to-image diffusion models. In *ICCV*, 2023. 1, 3, 4
- [44] Guosheng Zhao, Chaojun Ni, Xiaofeng Wang, Zheng Zhu, Guan Huang, Xinze Chen, Boyuan Wang, Youyi Zhang, Wenjun Mei, and Xingang Wang. Drivedreamer4d: World models are effective data machines for 4d driving scene representation. *arXiv preprint arXiv:2410.13571*, 2024. 2
- [45] Guosheng Zhao, Xiaofeng Wang, Zheng Zhu, Xinze Chen, Guan Huang, Xiaoyi Bao, and Xingang Wang. Drivedreamer-2: Llm-enhanced world models for diverse driving video generation. *arXiv preprint arXiv:2403.06845*, 2024. 2, 3
- [46] Zangwei Zheng, Xiangyu Peng, Tianji Yang, Chenhui Shen, Shenggui Li, Hongxin Liu, Yukun Zhou, Tianyi Li, and Yang You. Open-sora: Democratizing efficient video production for all, 2024. 1, 2, 3, 4, 6
- [47] Ziyang Zheng, Ruiyuan Gao, and Qiang Xu. Non-cross diffusion for semantic consistency. In *WACV*, 2025. 2
- [48] Brady Zhou and Philipp Krähenbühl. Cross-view transformers for real-time map-view semantic segmentation. In *CVPR*, 2022. 5

# MagicDriveDiT: High-Resolution Long Video Generation for Autonomous Driving with Adaptive Control

## Supplementary Material (Appendix)

Please find the videos on our project website: <https://flymin.github.io/magicdrivedit/>

**Note:** Our model is capable of generating videos at a resolution of  $848 \times 1600$  for 241 frames, which is the highest resolution and frame count in the nuScenes dataset. However, the inference cost is currently substantial. Therefore, the primary numerical results in our paper do not utilize this maximum setting. We have included some generated results in Appendix J and on our project website for reference. Future work may focus on further reducing the inference cost.

### A. Sequence Parallel Training

Inspired by Zheng et al. [46], we employ sequence parallelism to train DiT models with large sequence lengths. As illustrated in Figure I, we partition each input across the spatial dimension onto different GPUs. Most operations can be executed within a single GPU; however, the attention blocks necessitate communication. On the right side of Figure I, we demonstrate the communication process, where the full sequence is gathered, but the attention heads are distributed across different GPUs. This approach allows for peer-to-peer communication between GPUs while maintaining a roughly equal load.

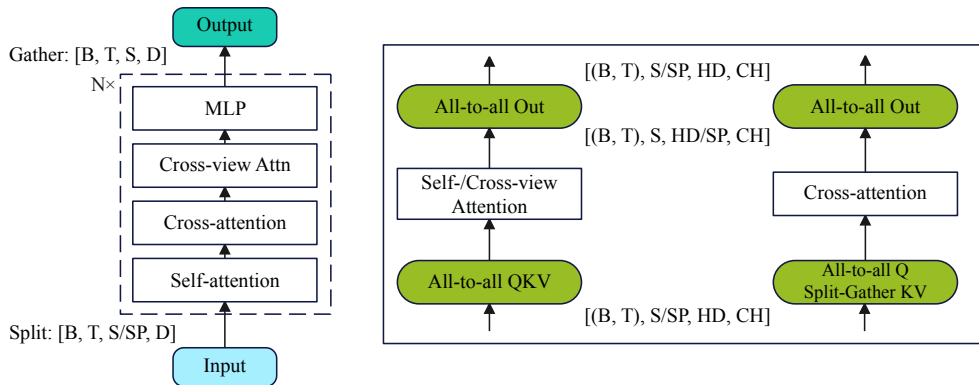


Figure I. **Diagram for Sequence Parallel.** *Left:* We split the spatial dimension before the first block and gather them after the last block. *Right:* For each attention module, we use all-to-all communication, changing the splitting dimension to attention heads. B: batch; T: temporal dimension; S: spatial dimension; D: latent dimension; HD: number of heads; CH: per-head dimension; SP: sequence parallel size.

Additionally, for VAE encoding and decoding, we partition based on batch size and the number of camera views, leveraging multiple GPUs to accelerate processing.

### B. More Details for Mixed Resolution and Frames Training

*MagicDriveDiT* is trained through a progressive training approach with variable length and resolution data configurations (see Section 4.5). Consequently, our method of data mixing corresponds to the three training stages, as detailed in Table I.

Inspired by [46], to maximize the utilization of GPU resources, we employed a bucket-like approach to adjust the data composition. Specifically, each GPU process (or sequence parallel communication group) loads only one type of data to ensure alignment of the batch dimension. Using the training time of the video format with the longest iteration time at batch size = 1 as a benchmark, we adjusted the batch sizes of other data formats so that each type runs at approximately the same speed. Notably, during stage 3 training, due to the limited number of full video clips, we repeat this type of data within an epoch. This ensures that different types of data have a similar magnitude of batch numbers within an epoch.

### C. Efficiency of Progressive Bootstrap Training

The three-stage progressive training approach markedly improves model training efficiency relative to direct Stage 3 training. Table II indicates that, over 4 days, for example, Stage 1 executes approximately 60 times more iterations than Stage 3, and

Stage	Resolution	Frame(s)	Sequence Parallel	Training Step
Stage 1	224×400	Img	-	80000
Stage 2	224×400 424×800	Img, 9, 17, 33, 65 Img, 9, 17, 33	-	40000
Stage 3	224×400 424×800 848×1600	Img, 17, full Img, 17, 33, 65, 129 Img, 9, 17, 33	4	30000

Table I. **Configuration for Variable Length and Resolution Training.** The mixing configuration aligns with our progressive bootstrap training with 3 stages, from low-resolution images to high-resolution long videos.

Stages	Seconds/Iter.	Iter. for 4 days
stage 1	4.32	80k
stage 2	39.84	8.7k
stage 3	*264.96	1.3k

Table II. **Speed for Each Training Stage of *MagicDriveDiT*,** measured on NVIDIA A800 GPUs. Over a 4-day period (for example), Stage 1 training yields nearly 60 times more iterations than Stage 3, and Stage 2 offers about 7 times more. \*This value is calculated by multiplication with sequence parallel (SP) size (in practice, we use SP size of 4 for the stage 3, with 66.24s/it).

Stage 2 achieves about 7 times more iterations. The progressive training is vital for controlled generative models, which require extensive iterations for effective convergence, as discussed in Section 4.5. The progressive strategy enables the rapid acquisition of high-quality video generation capabilities, utilizing faster iterations in the early stages to enhance convergence and expedite learning.

## D. More Experimental Details

The nuScenes [4] dataset includes 12Hz unannotated data and 2Hz annotated data. According to our experiments, high-frame-rate videos are more beneficial for generative model learning. Therefore, we follow [11] and interpolated the 2Hz annotations to 12Hz annotations with ASAP [36]. Although the interpolation results are not entirely accurate, they do not affect the training for video generation. The Waymo Open Dataset [33] includes 10Hz annotated data. We follow the official splitting, which has 798 clips for training and 202 clips for validation. The original dataset contains 5 views. However, the dimensions of the left and right side views are smaller than those of the three front views, and their field of view is limited. Therefore, we only retain three front views for training and validation.

**Semantic Classes for Generation.** We follow [11] in data setup on nuScenes. Specifically, for objects, ten categories include car, bus, truck, trailer, motorcycle, bicycle, construction vehicle, pedestrian, barrier, and traffic cone. For the road map, eight categories include drivable area, pedestrian crossing, walkway, stop line, car parking area, road divider, lane divider, and roadblock. For Waymo, the semantics for objects include pedestrian, car, and cyclist, while the semantics for road maps include drivable area, crosswalk, road line (yellow), and road line (white).

## E. More Training Details

**Optimization.** We train our diffusion models using Adam optimizer and a constant learning rate at  $8e^{-5}$  with a 3000-step linear warm-up in the last two stages. We primarily use 32 NVIDIA A800 GPUs (80G) for training. Our model can also be trained with Ascend 910B (64G). The batch size for each stage is set according to the iteration speed, following the bucket strategy as [46]. For example, in stage 2, we set the batch size for  $33 \times 424 \times 800$  to 1, which takes about 30s/it. Then we set the batch size to other video types to achieve about 30s/it. This strategy can ensure the load balance between different GPU processes.

**Inference.** By default, images/videos are sampled using Rectified Flow [9] with 30 steps and the classifier-free-guidance (CFG) scale at 2.0. To support CFG, we randomly drop different conditions at a rate of 15%, including embeddings for text, camera, ego trajectory, and boxes. We follow Gao et al. [11] to use  $\{0\}$  as the *null* condition for maps in CFG inference. When inferring high-resolution long videos, we also use sequence parallel (Appendix A) to fit in the limited memory of a single GPU.

## F. Human Evaluation for Multi-frame & Multi-view Consistency

Evaluating multi-frame and multi-view consistency in video generation has long been a challenging issue [1], as the academic community lacks a unified standard to accurately assess such consistency. To address this, we employed human evaluation to measure these two aspects of consistency. Specifically, we invited participants with diverse backgrounds to compare videos generated by *MagicDriveDiT* and Gao et al. [11] under identical conditions. Participants were asked to select the video with better consistency, and the winning probability of each model was statistically analyzed. As illustrated in Figure II, *MagicDriveDiT* demonstrated significantly superior consistency, indicating a substantial improvement over Gao et al. [11].

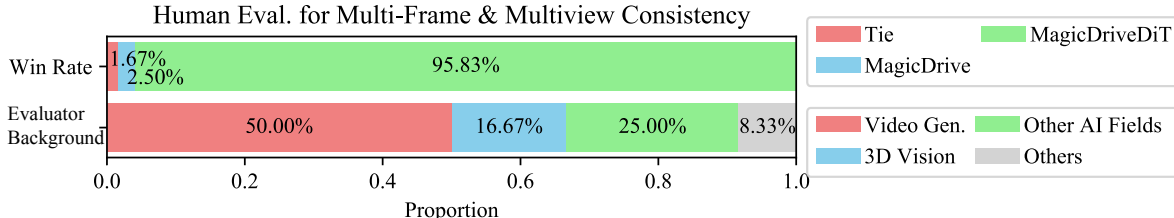


Figure II. Experts evaluated content consistency against Gao et al. [11], showing *MagicDriveDiT* generates videos with superior consistency.

## G. More Comparison among VAEs

To quantitatively compare the performance of the VAE, we randomly selected two 6-view videos from the nuScenes dataset and used the PSNR metric to evaluate the VAE’s reconstruction ability. Table III presents the results, averaged across the six views. From these results, we observe that CogVAE [42] demonstrates the best reconstruction ability, even surpassing the 2D VAE [30]. Comparing the results from different settings, we find that the current 3D VAEs exhibit good generalization ability for long videos, primarily due to the window-based downsampling techniques [42, 46]. Additionally, we observe that high-resolution content retains a relatively high PSNR after VAE reconstruction, indicating that the current VAEs are more favorable for high-resolution data. This observation also supports our motivation for high-resolution generation.

Resolution	Model	Image	17 fr.	33/34 fr.
224×400	CogVAE	<b>34.4261</b>	<b>31.0900</b>	<b>30.5986</b>
	Open-Sora	30.4127	27.9238	27.5245
	SD VAE	27.7131	27.7593	27.9404
424×800	CogVAE	<b>38.4786</b>	<b>33.5852</b>	<b>32.9202</b>
	Open-Sora	33.6114	30.2779	29.8426
	SD VAE	30.9704	31.0789	31.3408
848×1600	CogVAE	<b>41.5023</b>	<b>36.0011</b>	<b>35.1049</b>
	Open-Sora	37.0590	33.2856	32.8690
	SD VAE	37.0504	33.2846	32.8680

Table III. **VAE Comparison for Street Views.** CogVAE [42] and Open-Sora [46] (1.2) are 3D VAEs; SD VAE [30] is 2D VAE, which is also widely adopted by previous street view generation (e.g., [11]). Results are PSNRs calculated through videos from the nuScenes validation set. *MagicDriveDiT* adopts CogVAE.

## H. Reason for Using CogVAE without the Pre-trained Diffusion Model

Informed by the work of MagicDrive [11] and others [12], fine-tuning from a well-performing diffusion model can effectively accelerate model convergence. Consequently, in the initial implementation of the DiT architecture, we experimented with Open-Sora 1.2 [46]’s VAE and diffusion models. However, the results were suboptimal, with image generation and video controllability falling short of MagicDrive’s performance. We attribute this primarily to the limited generalization capability of text-to-video diffusion and, more critically, to the inadequate reconstruction ability of the VAE.

We conducted a comparative analysis of VAEs, as detailed in Section 5.3 and Appendix G, and found CogVAE [42] to perform well. Given that the VAE determines the upper limit of generation quality, we opted to use CogVAE for video

encoding. Notably, CogVideoX [42] employs a novel DiT structure, where each layer’s latent space integrates both video and text condition information. This approach may complicate the design of geometry-related conditions. Furthermore, CogVideoX was not trained in a driving scenario. To eliminate these potential confounding factors, we decided to train the diffusion model from scratch using CogVAE. This strategy allows us to move beyond the constraints of pre-trained models, enabling more flexible modifications to the model architecture to achieve multi-view consistency and spatiotemporal encoding of geometry conditions.

Our experience directly demonstrates that high-resolution, long street-view video generation does not necessarily require pre-trained image-text or video-text models. Even so, this is beyond the primary focus of our paper, and we leave related questions for future work.

## I. Single Inference v.s. Rollout Inference



(a) **Generation from Vista.** It takes the first frame as input and generates the following (only supporting the front view).



(b) **Generation from *MagicDriveDiT*.** We take conditions as inputs and generate the full video (only show the first 9s for comparison).

Figure III. **Comparison between Rollout for Long Videos (Vista [12]) and Single Inference (our *MagicDriveDiT*).** Although rollout can handle long videos, the quality is significantly degraded. In contrast, our extrapolation maintains high quality in long video generation.

To achieve long video generation, previous work typically employs a method of future frame prediction combined with rollout. This involves, after the  $n$ -th inference, taking the last  $l$  frames from this inference as the first  $l$  frames for the  $n + 1$ -th inference, thus enabling long video generation. However, since the model does not directly capture long-term dependencies and accumulates errors with each inference, such rollouts often fail to support sufficiently long videos. Among rollout methods, Vista [12] currently achieves relatively good results. We compared a 9-second video generated by performing 4 rollouts with Vista (the paper claims it can support 6 rollouts) to a 9-second segment produced by our method, *MagicDriveDiT*. It is evident that our method maintains consistent video quality over long sequences, whereas Vista’s results show a noticeable decline. Therefore, we believe that the hybrid training and length extrapolation approach adopted by *MagicDriveDiT* can achieve higher quality in long video generation.

## J. More Visualization

As said in the “Note”, *MagicDriveDiT* is capable of generating  $6 \times 848 \times 1600 \times 241$  videos (20s at 12 fps). We include more generated samples in Figure IV-V. Please see the videos on our project page.

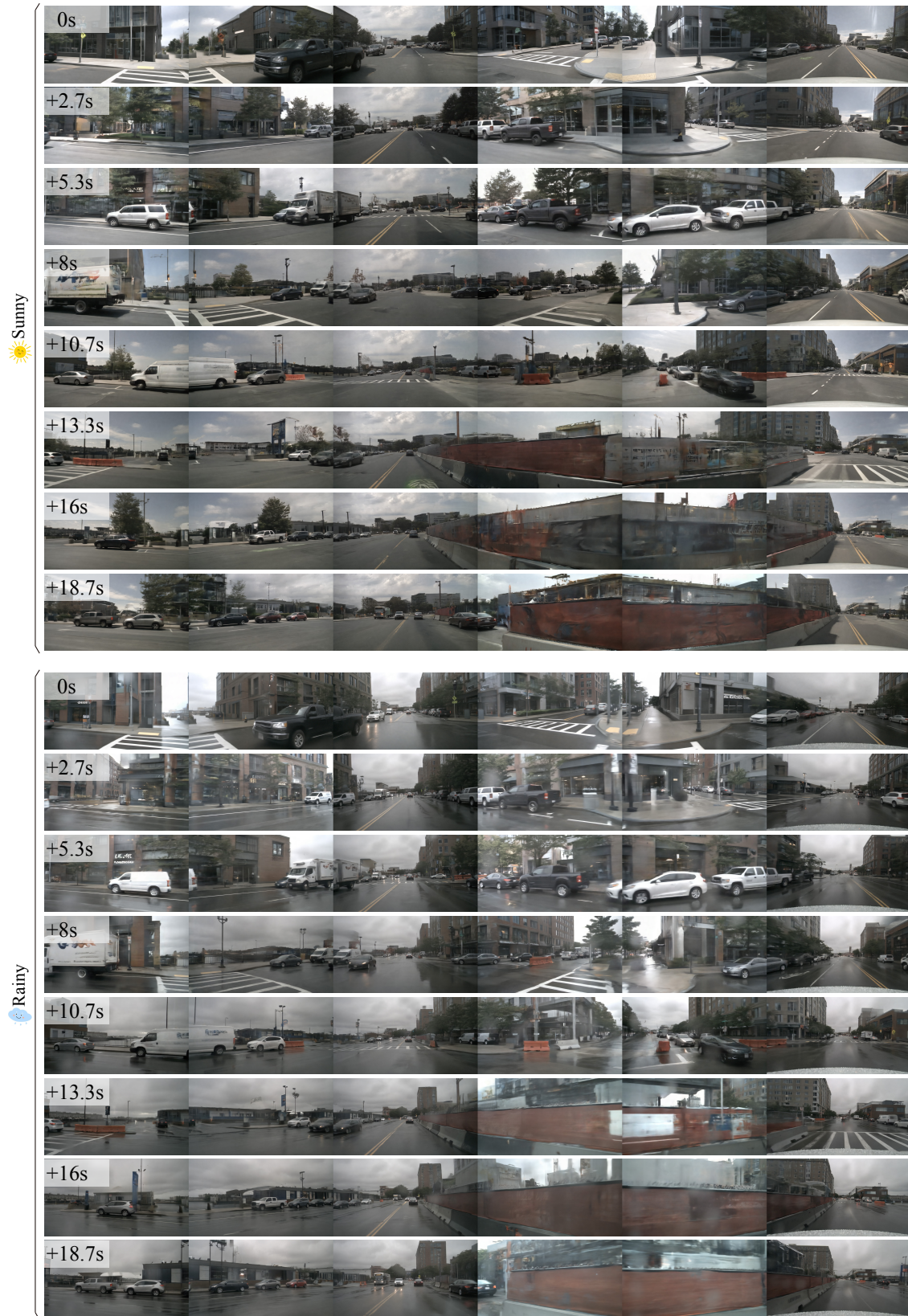


Figure IV. We show some frames from the generated  $6 \times 848 \times 1600 \times 241$  videos with the same scene configuration (*i.e.*, boxes, maps, cameras, and ego trajectory) but under different weather conditions. Conditions are from the nuScenes validation set.

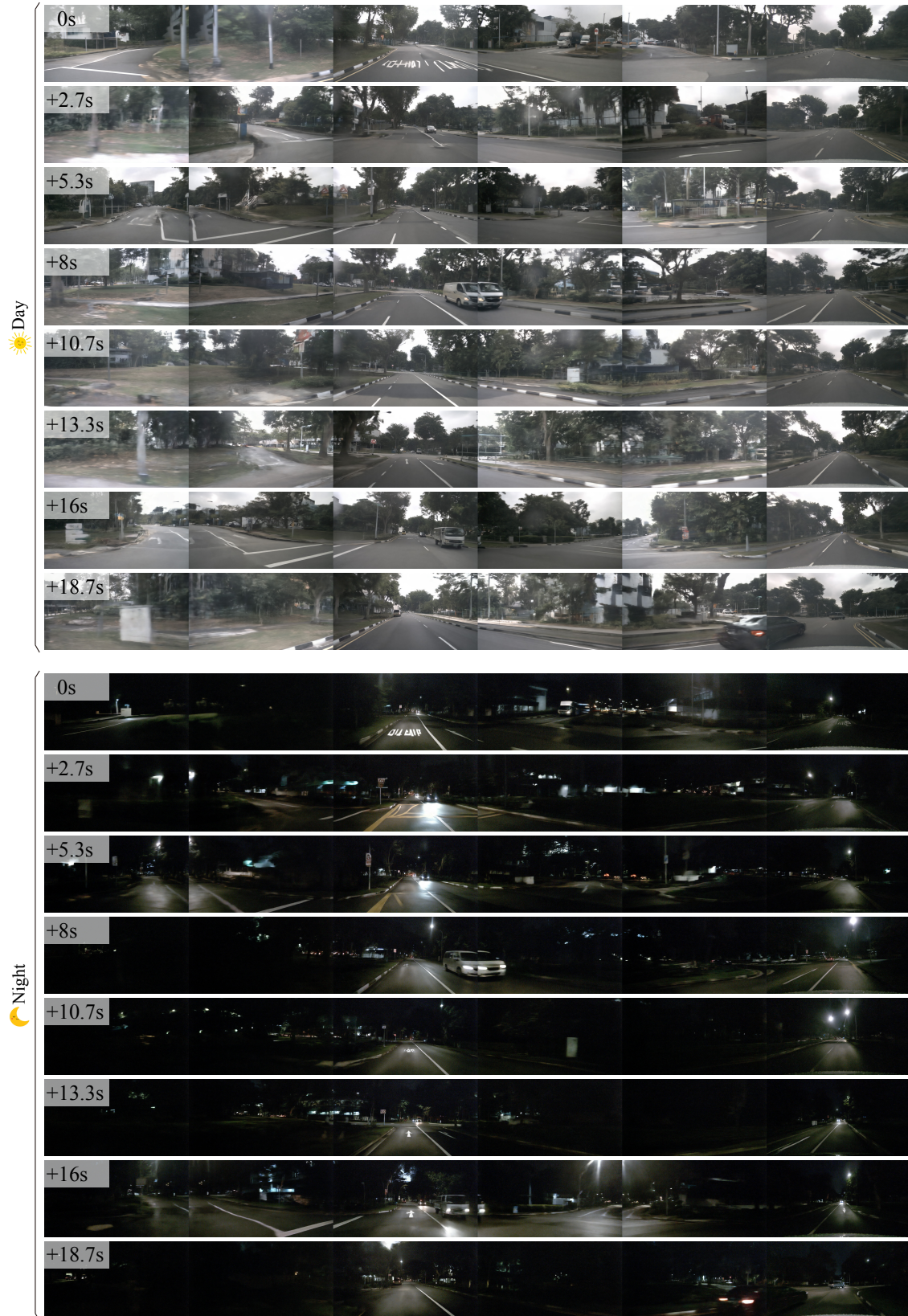


Figure V. We show some frames from the generated  $6 \times 848 \times 1600 \times 241$  videos with the same scene configuration (*i.e.*, boxes, maps, cameras, and ego trajectory) but under different time-of-day conditions. Conditions are from the nuScenes validation set.